Investigation of the mechanism of polarization switching in ferroelectric capacitors by three-dimensional piezoresponse force microscopy

B. J. Rodriguez, A. Gruverman,[a)] A. I. Kingon, R. J. Nemanich,
North Carolina State University, Raleigh, NC 27695, USA
and
J. S. Cross
Fujitsu Laboratories Ltd, Atsugi 243-0197, JAPAN

A mechanism of the switching behavior of (111)-oriented $Pb(Zr,Ti)O_3$-based 1x1.5 μm^2 capacitors has been investigated using three-dimensional piezoresponse force microscopy (3D-PFM). A combination of vertical and lateral piezoresponse force microscopy (VPFM and LPFM, respectively) has been used to map the out-of-plane and the in-plane components of the polarization. The three-dimensional polarization distribution was reconstructed by quantitative analysis of the PFM *amplitude* images of poled PZT capacitors while taking into account contrast variations in the PFM *phase* images. The switching behavior of the capacitors was determined by comparison of the static domain patterns in the same capacitors after both positive and negative poling. While 180º degree switching was observed, surprisingly, the switching process was dominated by 90º polarization vector rotation. Furthermore, central regions of the capacitors were characterized by the presence of charged domain boundaries, which could lead to imprint.

[a)] E-mail address: alexei_gruverman@ncsu.edu

I Introduction

As the integration density of ferroelectric random access memory (FRAM) continues to increase, understanding the switching behavior of constituent microcapacitors becomes more important for addressing the reliability issues of FRAM devices [1]. Piezoresponse force microscopy (PFM) has demonstrated the capacity for direct, non-destructive, high-resolution characterization of the properties of ferroelectric thin films and capacitors, including their switching behavior at the nanoscale [2-14]. It has also proved to be a powerful tool for studying the mechanisms of various degradation effects in ferroelectrics. Recently, it has been demonstrated that PFM is capable of discerning the in-plane and out-of-plane components of polarization, which has allowed complete reconstruction of the three-dimensional polarization in ferroelectric thin films and capacitors [15-21]. Development of this method, termed three-dimensional PFM (3D-PFM), provides a method for better understanding the underlying mechanisms of nanoscale ferroelectric behavior. For example, the three-dimensional reconstruction of polarization allowed observation of charged domain walls in the bulk of the ferroelectric capacitors, which could contribute to the imprint (preference of one polarization state over another) [22] behavior of ferroelectric capacitors.

In this paper, we have used 3D-PFM to study a mechanism of polarization switching in ferroelectric capacitors by monitoring the changes in their domain structures after voltage application. Furthermore, we present quantitative analysis of the PFM amplitude images based on the full piezoelectric tensor of the tetragonal PZT films. It is demonstrated that 3D-PFM may provide further insight into imprint behavior of ferroelectric capacitors.

2 Experimental Details

In this study, 200 nm thick layers of tetragonal (111)-fiber textured PZT were deposited onto a Pt bottom electrode. Transmission electron microscopy (TEM) revealed a columnar grain structure with an average PZT grain size of approximately 200 nm. Reactive ion etching was used to fabricate 1x1.5-μm^2 capacitors with 50 nm thick IrO_2 top electrodes on the PZT surface. The PZT surface was etched 40 nm below the top electrode/PZT interface, leaving PZT capacitor islands. VPFM and LPFM imaging methods, used to detect out-of-plane and in-plane polarization components, respectively, have been described in detail elsewhere [2-21]. The modulation voltage (0.6 Vrms at 10 kHz) was applied to the top electrode of the capacitor using a conductive PFM tip, which was also used to detect the piezoelectric response of the capacitor. A voltage of +/- 5 V was applied for 3 seconds to the top electrode in order to switch the capacitor to a negative or positive state, respectively. Three-dimensional reconstruction was performed on an array of 8 capacitors, however, 3D-PFM images from one representative capacitor are shown in this paper. Commercially available Pt coated Si rectangular cantilevers (1.0-2.6 N/m force constant) have been used in this study.

In PFM, an ac voltage applied between the probing tip and sample results in a sample surface vibration due to the converse piezoelectric effect. This vibration, transmitted via the elastic deformation and friction forces into the vertical oscillation and torsional movement of the cantilever, is detected using a lock-in technique. The perpendicular cantilever displacement is associated with out-of plane polarization (VPFM), while the lateral vibration (torsion) is related to in-plane polarization (LPFM). In a situation where the applied field is parallel to the polar axis of a tetragonal

ferroelectric sample, the VPFM amplitude signal is proportional to the d_{33} piezoelectric coefficient and interpretation of VPFM images is rather straightforward [5]. However, if the polarization vector is oriented at some angle to the film plane, the measured piezoelectric coefficient d_{zz} (the constant measured along the direction normal to the surface) is not equal to d_{33} nor is it proportional to the spontaneous polarization [23-27]. In this case, in order to quantify the VPFM signal and to obtain correct information on polarization orientation it is necessary to take into account a complete piezoelectric tensor of the material under investigation and calculate its components in a laboratory system of coordinates.

In general, for an arbitrarily rotated grain, the components of the piezoelectric tensor transform as [28]

$$d_{ijk} = A_i^m A_j^n A_k^l d_{mnl}^0, \tag{1}$$

where A is given by

$$A_i^j = a_{ij} = x_i x_j, \tag{2}$$

and x_i and x_j are orthonormal bases representing a new and the original coordinate system, respectively.

The transformed piezoelectric tensor in reduced tensor notation for tetragonal thin films can be written as

$$\begin{bmatrix} 0 & 0 & 0 & 0 & d_{15}\cos\theta & d_{15}\sin\theta \\ d_{31}\sin\theta & \begin{matrix}(d_{31}+d_{15})\sin\theta\cos^2\theta \\ +d_{33}\sin^3\theta\end{matrix} & \begin{matrix}(d_{33}-d_{15})\sin\theta\cos^2\theta \\ +d_{31}\sin^3\theta\end{matrix} & \begin{matrix}2(d_{33}-d_{31})\sin^2\theta\cos\theta \\ +d_{15}\cos\theta(\cos^2\theta-\sin^2\theta)\end{matrix} & 0 & 0 \\ d_{31}\cos\theta & \begin{matrix}(d_{33}-d_{15})\sin^2\theta\cos\theta \\ +d_{31}\cos^3\theta\end{matrix} & \begin{matrix}(d_{31}+d_{15})\sin^2\theta\cos\theta \\ +d_{33}\cos^3\theta\end{matrix} & \begin{matrix}2(d_{33}-d_{31})\sin\theta\cos^2\theta \\ -d_{15}\sin\theta(\cos^2\theta-\sin^2\theta)\end{matrix} & 0 & 0 \end{bmatrix} \tag{3}$$

Hence, for tetragonal thin films, the effective piezoelectric constant d_{zz}, measured as the VPFM amplitude, is given by

$$d_{zz}(\theta) = (d_{31} + d_{15})\sin^2\theta\cos\theta + d_{33}\cos^3\theta \quad (4)$$

where θ is the angle between the measurement direction and the [001] crystallographic axis [28]. An important consequence of this result is that the measured piezoresponse will depend on the d_{33}, d_{31} and d_{15} piezoelectric coefficients, as described elsewhere [27].

In LPFM, the modulation voltage is still applied along the z-axis, however the strain is measured along the x- or y-direction. The amplitude of the lateral vibration is linked to the in-plane component of polarization via the combination of piezoelectric coefficients. As can be seen in the expression for the transformed tensor (Equation (3)), the effective piezoelectric constants d_{zx} and d_{zy} , measured as the LPFM amplitudes, for tetragonal thin films are given by

$$d_{zx}(\theta) = d_{31}\cos\theta \quad (5)$$

$$d_{zy}(\theta) = (d_{33} - d_{15})\sin^2\theta\cos\theta + d_{31}\cos^3\theta \quad (6)$$

where θ is the angle between the direction normal to the film plane and the [001] crystallographic axis.

Shown in Fig. 1 are the cross-sections of the d_{zx}, d_{zy} and d_{zz} piezoelectric surfaces by the (010) plane for a tetragonal PZT film. Calculations have been made using the following thin film values for the piezoelectric coefficients: d_{31}=-59 pm/V, d_{15}=169 pm/V d_{33}=162 pm/V [29]. Calculations of the d_{zx}, d_{zy} and d_{zz} constants have been performed for the (111)-oriented grain (measurement direction coincides with the [111] axis). Strictly speaking, LPFM is a measurement of d_{zx} and d_{zy} where d_{zx} and d_{zy} are proportional to the

projection of their piezoelectric surfaces onto the x-y plane. However, since the projection of d_{zz}, which also includes an in-plane component of polarization in (111) PZT, is much larger than the d_{zx} or d_{zy} projections, only d_{zz} need be considered.

In the case of the tetragonal PZT unit cell, there are 6 possible orientations of the polarization vector, half of which are related by inversion along the pseudocubic principal crystallographic axes. With regards to VPFM, there are two sets of opposite polarization directions that can be distinguished by detecting the phases of the first harmonic signals (they differ by 180º). On the other hand, in LPFM, projections of all 6 possible polarization directions on the x-y plane can be distinguished, as discussed in Ref. 19. Note that in this case, detection of both amplitude and phase signals is necessary to determine the actual polarization direction. For the case of a poled capacitor with domains that extend from the bottom electrode to the top electrode (through domains), the direction of the out-of-plane polarization component can be unequivocally determined by VPFM and this leaves only 3 possible orientations of in-plane polarization, each separated by 120º. Hence, the interpretation of LPFM data becomes more direct. Reconstruction of the polarization vector in ferroelectric capacitors has been discussed in detail in Ref.20.

3 Results

In Figs. 2(a, d) VPFM amplitude and phase images are shown for a 1×1.5-μm^2 capacitor poled with a ***negative*** bias. Regions in the VPFM phase image (Fig. 2(d)) that have dark contrast represent positive domains (normal component of polarization oriented upward), while bright regions represent negative domains. As previously reported, there are

spatial variations in the VPFM amplitude signal across the top electrode of the capacitor [11,12]. Figures 2(b, e) show LPFM amplitude and phase images, respectively, of the same capacitor, while Figs. 2(c, f) show LPFM amplitude and phase images, respectively, of the same capacitor after its counter-clockwise rotation of 90º with respect to the measurement direction (normal to the film plane).

In Figs. 3(a, d) VPFM amplitude and phase images are shown for the same 1×1.5-μm^2 capacitor as in Fig.2 but poled with a ***positive*** bias. Figures 3(b, e) show LPFM amplitude and phase images, respectively, of the same capacitor, while Figs. 3(c, f) show LPFM amplitude and phase images of the rotated capacitor, respectively.

In Fig. 4, the three-dimensional polarization distribution for the negatively and positively poled capacitors in Figs. 2 and 3 are reconstructed based on their VPFM phase images (Figs. 4(a, b)) and maps of the in-plane polarization (Figs. 4(c, d)) determined from LPFM-X and LPFM-Y data. Fig. 4(e) shows the x-y projections of three d_{zz} piezoelectric surfaces for both negatively (black arrows) and positively poled capacitors (gray arrows). In Fig. 4(f), the pseudocubic principal crystallographic axes are shown for clarity.

It should be emphasized that a single crystalline approximation used to determine the three-dimensional polarization orientation from PFM data of the polycrystalline PZT capacitors produces satisfactory results. This may be explained by the presence of multiple nucleation sites on single Pt grains of the bottom electrode, which can result in a capacitor in which the PZT has predominantly a single crystallographic orientation (including in-plane). TEM analysis supports this assumption by revealing Pt grains larger than the average PZT grain. In this case, texturing, with low angle grain boundaries at the submicron scale, could be well described using the single crystalline approximation. Note, however, that the white

arrow in Fig. 4(d) corresponds to a domain that does not fit the proposed piezoelectric surface cross-section, suggesting the presence of a high angle grain boundary in this particular location. A portion of the capacitor therefore has a different in-plane crystallographic orientation, while retaining the same out-of-plane orientation of the poled capacitor. Thus, the 3D reconstruction has to be performed with great care.

4 Discussion

Now let us discuss the main outcome of these results, namely, the mechanism of ferroelectric switching in micrometer scale capacitors. As will be shown below, this mechanism involves both 180º and 90º domain switching.

Whereas the presence of the top electrode made it difficult to distinguish between 90º and 180º domain walls near regions of opposite VPFM phase in poled capacitors [20], with three-dimensional reconstruction of polarization in both polarization states, it is possible to determine the type of polarization reconstruction in the capacitor, i.e. whether it is 180º switching or 90º rotation of the polarization vector. While care is taken to reconstruct domain boundaries that are consistent with allowable domain walls, we are limited by the presence of the top electrode and cannot unequivocally distinguish between domain walls and grain boundaries. For instance, in the upper right quadrant of the capacitor in Fig. 4(c, d), the polarization switches from the [010] direction to the $[0\bar{1}0]$ direction, which suggests 180º domain switching. This 180º domain switching is illustrated in isometric projection in Figs. 5(a, b). It is generally expected that only 180º domain switching would occur in PZT capacitors since ferroelastic 90º domain walls should be immobile as a result of substrate clamping [30]. In the case of our PZT capacitors, however, it is quite clear

that much of the capacitor switches by 90º as seen in Figs 4(c, d). In particular, the lower left quadrant of the capacitor in Fig. 4(c, d) is an example of 90º polarization rotation from the [010] direction to the $[\bar{1}00]$ direction. This 90º domain switching is illustrated in an isometric projection in Figs. 6(a, b). Analysis of switching in an array of 8 capacitors revealed that 90º switching is predominant in 1x1.5 μm^2 capacitors. Ninety degree domain switching is most likely enabled by the strain relief caused by etching. As reported by V. Nagarajan *et al.*, 90º domain wall motion has also been observed in FIB-patterned PZT islands [31].

The boundary between head-to-head or tail-to-tail polarization regions carries a large electrostatic penalty. Nevertheless, these charged boundaries are present in the poled capacitor. Note that in the center of the capacitor in Fig. 4(d), there is a charged 180º domain boundary with a head-to-head domain configuration. It can be seen in Figs. 5(a, b) that 90º domain walls can also carry polarization screening charges. The presence of these charged boundaries is indisputable evidence there is a source of available charge. Oxide electrodes are thought to provide a source of charge and have higher leakage characteristics than Pt electrodes [32]. Accumulation and trapping of the electronic charge at the charged domain walls can be a significant source of imprint [22] as has been observed in the central regions of similar PZT capacitors [11].

In our previous study [11], we found that inner regions of the capacitors are negatively imprinted and tend to switch back after being poled by a positive bias, while regions at the edge of the capacitors tend to exhibit more symmetric hysteresis behavior. We attributed these spatial variations to a combination of mechanical stress and electrical field effects [11]. It is interesting to note that non-switching (or backswitching) [11] regions in

Figs. 4(c) (represented by gray arrow) and 4(d) (represented by black arrow) also lie in the central regions of the capacitor. In fact, these non-switching regions provide evidence of domain pinning since they are adjacent non-switching regions marked by reduced piezoresponse magnitude (Figs. 2(a, d) and 3(a, d)). Not only are the out-of-plane components of polarization for these regions pinned, but so are the in-plane components, as demonstrated by three-dimensional reconstruction of the polarization before and after switching (Figs. 4(c, d)). This is further evidence of the presence of a complex combination of mechanical stress and electrical field effects. Furthermore, as can be seen in the VPFM amplitude image of the capacitor poled with a negative bias (Fig. 2(a)) there appears to be domain boundaries running along the capacitor edge that are not present in the VPFM amplitude image of the capacitor poled with a positive bias (Fig. 3(a)). These boundaries separate the edge regions with positive out-of-plane polarization from the capacitor interior with negative polarization and demonstrate spatial variations in the domain patterns.

5 Summary

3D-PFM has been used to map the domain orientation of the underlying PZT thin film of (111)-oriented 1x1.5 μm^2 PZT capacitors after both positive and negative poling to investigate a mechanism of switching behavior in ferroelectric capacitors. A combination of vertical and lateral piezoresponse force microscopy (VPFM and LPFM, respectively) has been used to map the out-of-plane and the in-plane components of polarization after both positive and negative poling. The three-dimensional polarization distribution was reconstructed by quantitative analysis of the PFM amplitude images of poled capacitors while taking into account contrast variations in the PFM phase images. It was found that 90º

switching is dominant in (111)-oriented tetragonal PZT capacitors and that 180º switching generally occurs near the capacitor edge, which exhibits symmetric hysteresis behavior. Central regions of the capacitors, which have also been shown to be imprinted, were characterized by charged domain walls as evidenced by the presence of pinned domains. The role of imprint on switching behavior may be further addressed by 3D-PFM in combination with optical/thermal treatment of capacitors.

Acknowledgements

The authors are grateful to Dr. S. V. Kalinin and Dr. A. Pignolet for discussions related to piezoelectric surfaces. This study is supported by the National Science Foundation (Grant No. DMR-0235632) and Fujitsu Limited.

References

1 U. Böttger, S. R. Summerfelt, in Nanoelectronics and Information Technology, edited by R. Waser (WILEY-VCH, Weinheim, 2003), Chap. 22, pp. 567-588

2 A. Gruverman, O. Auciello, and H. Tokumoto, Appl. Phys. Lett. **69**, 3191 (1996)

3 S. V. Kalinin and D. A. Bonnell, Phys. Rev. **B 65**, 125408 (2002)

4 A. Gruverman, O. Auciello, and H. Tokumoto, Annu. Rev. Mater. Sci. **28**, 101 (1998)

5 J. A. Christman, R. R. Woolcott, A. I. Kingon, and R. J. Nemanich, Appl. Phys. Lett. **73**, 3851 (1998)

6 J. A. Christman, S.-H. Kim, H. Maiwa, J.-P. Maria, B. J. Rodriguez, A. I. Kingon, and R. J. Nemanich, J. Appl. Phys. **87**, 8031 (2000)

7 A. Gruverman, B. J. Rodriguez, R. J. Nemanich, and A. I. Kingon, J. Appl. Phys. **92**, 2734 (2002)

8 M. Alexe, A. Gruverman, C. Harnagea, N. D. Zakharov, A. Pignolet, D. Hesse and J. F. Scott, Appl. Phys. Lett. **75**, 1158 (1999)

9 M. Alexe, C. Harnagea, D. Hesse, and U. Gösele, Appl. Phys. Lett. **79**, 242 (2001)

10 I. Stolichnov, E. Colla, A. Tagantsev, S. Bharadwaja, S. Hong, N. Setter, J. S. Cross, and M. Tsukada, Appl. Phys. Lett. **80**, 4804 (2002)

11 A. Gruverman, B. J. Rodriguez, A. I. Kingon, R.J. Nemanich, J.S. Cross, and M. Tsukada, Appl. Phys. Lett. **82**, 3071 (2003)

12 A. Gruverman, B. J. Rodriguez, A. I. Kingon, R. J. Nemanich, A.K. Tagantsev, J. S. Cross, M. Tsukada, Y. Horii, Appl. Phys. Lett. **83,** 728 (2003)

13 L.M. Eng, H.-J. Güntherodt, G. Rosenman, A. Skliar, M. Oron, M. Katz, and D. Eger, J. Appl. Phys. **83**, 5973 (1998)

14 L. Chen, J. Ouyang, C. S. Ganpule, V. Nagarajan, R. Ramesh, and A. L. Roytburd, Appl. Phys. Lett. **84**, 254 (2004)

15 L.M. Eng, M. Abplanalp, P. Günter, Appl. Phys. A. **66**, S679-S683 (1998)

16 L. M. Eng, H. J. Güntherodt, G. A. Schneider, U. Köpke, and J. Muñoz Saldaña, Appl. Phys. Lett., **74** 233 (1999)

17 M. Abplanalp, L.M. Eng, P. Günter, Appl. Phys. A. **66**, S231-S234 (1998)

18 A. Roelofs, U. Böttger, R. Waser, F. Schlaphof, S. Trogisch, L.M. Eng, Appl. Phys. Lett. **77**, 3444 (2000)

19 C. S. Ganpule, V. Nagarajan, B. K. Hill, A. L. Roytburd, E. D. Williams, S. P. Alpay, A. Roelofs, R. Waser, and L.M. Eng, J. Appl. Phys. **91**, 1477 (2002)

20 B. J. Rodriguez, A. Gruverman, A. I. Kingon, R. J. Nemanich, and J. S. Cross, J. Appl. Phys. **95**, 1958 (2004)

21 A. Roelofs, N. A. Pertsev, R. Waser, F. Schlaphof, L. M. Eng, C. Ganpule, V. Nagarajan, R. Ramesh, Appl. Phys. Lett. **80**, 1424 (2002)

22 D. Dimos, W. L. Warren, M. B. Sinclair, B. A. Tuttle, and R. W. Schwartz, J. Appl. Phys. **76**, 4305 (1994)

23 X. Du, U. Belegundu, K. Uchino, Jpn. J. Appl. Phys. **36**, 5580 (1997)

24 X. Du, J. Zheng, U. Belegundu, K. Uchino,. Appl. Phys. Lett. **72**, 2421 (1998)

25 X. Du, Q.-M. Wang, U. Belegundu, A. Bhalla, K. Uchino, Materials Lett. **40**, 109 (1999)

26 S. Kalpat, X. Du, I.R. Abothu, A. Akiba, H. Goto and K. Uchino, Jpn. J. Appl. Phys. **40**, 713 (2001)

27 C. Harnagea, A. Pignolet, M. Alexe and D. Hesse, Integrated Ferroelectrics **38**, 23 (2001)

28 W.G. Cady, *Piezoelectricity*. Dover Publications, Inc., New York 1964

29 M. J. Haun, Ferroelectrics **99**, 63 (1989)

30 B. A. Tuttle, T. J. Gario, J. A. Voight, T. J. Headley, D. Dimos, M. O. Eatough, in Science and Technology of Electroceramic Thin films, edited by O. Auciello and R. Waser (Kluwer Academic Publishers, The Netherlands, 1995), pp. 117-132

31 V. Nagarajan, A. Roytburd, A. Stanishevsky, S. Prasertchoung, T. Zhao, L. Chen, J. Melngailis, O. Auciello And R. Ramesh, Nature Materials **2**, 43-47 (2003)

32 H. N. Al-Shareef, O. Auciello, A. I. Kingon, J. Appl. Phys. **77**, 2146 (1995)

Fig. Captions

Fig. 1 Cross-section of the d_{zx}, d_{zy} and d_{zz} piezoelectric surfaces by (010) plane for (111)-oriented tetragonal PZT film. Note that the angle between the measurement direction and the polarization direction is fixed.

Fig. 2 VPFM and LPFM images of (a, b) amplitude and (d, e) phase, respectively, of a negatively poled ferroelectric capacitor. LPFM (c) amplitude and (f) phase of the same capacitor following a 90º counter clockwise rotation of the sample.

Fig. 3 VPFM and LPFM images of (a, b) amplitude and (d, e) phase, respectively, of a positively poled ferroelectric capacitor. LPFM (c) amplitude and (f) phase of the same capacitor following a 90º counter clockwise rotation of the sample.

Fig. 4 (a, b) VPFM phase images of the negatively and positively poled (111) PZT ferroelectric capacitors, respectively. (c) Reconstruction of the in-plane polarization map of the negatively poled ferroelectric capacitor shown in Fig. 2. (d) Reconstruction of the in-plane polarization map of the positively poled ferroelectric capacitor shown in Fig. 3. (e) Projection of the piezoelectric surfaces onto the (111) plane for three possible in-plane polarization directions. Arrows indicate the direction of uniformly polarized regions and correspond to the x-y projection of the piezoelectric surfaces for both negative (black arrows) and positive out-of-plane polarization (gray arrows). The white arrow corresponds to a domain that does not fit the proposed piezoelectric surface cross-sections, which is

consistent with the fiber textured PZT structure. (f) The pseudocubic principal crystallographic axes are shown for clarity.

Fig. 5 Isometric projection of the reconstructed polarization (for a cross-section along line 1 in Figs. 4(c, d) after capacitor poling by negative (a) and positive (b) voltage. Note that the polarization of both regions switches by 180º following the application of a switching voltage.

Fig. 6 Isometric projection of the reconstructed polarization (for a cross-section along line 2 in Figs. 4(c, d) after capacitor poling by negative (a) and positive (b) voltage. Note that the polarization of the left side of the capacitor in Fig. 6(a) switches by 90º following the application of a switching voltage. This is indicative of 90º switching.

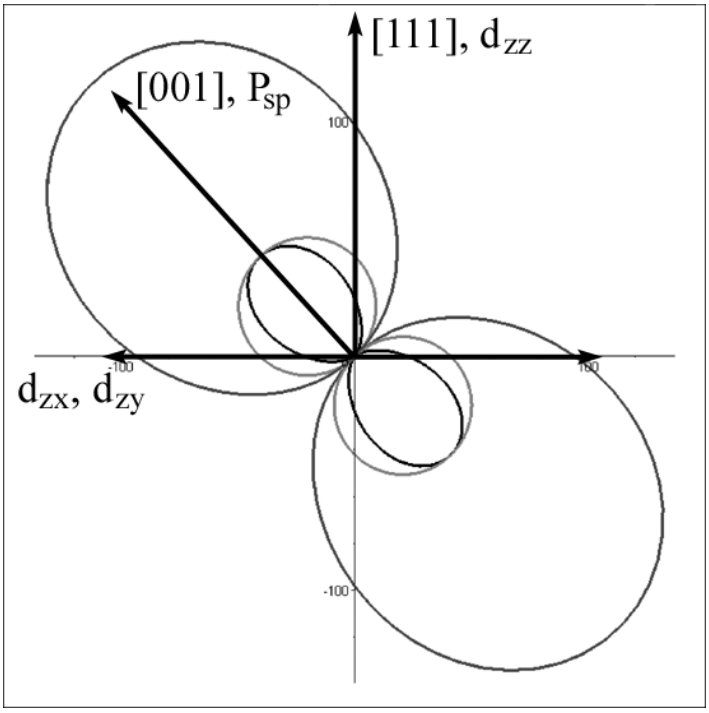

Fig. 1

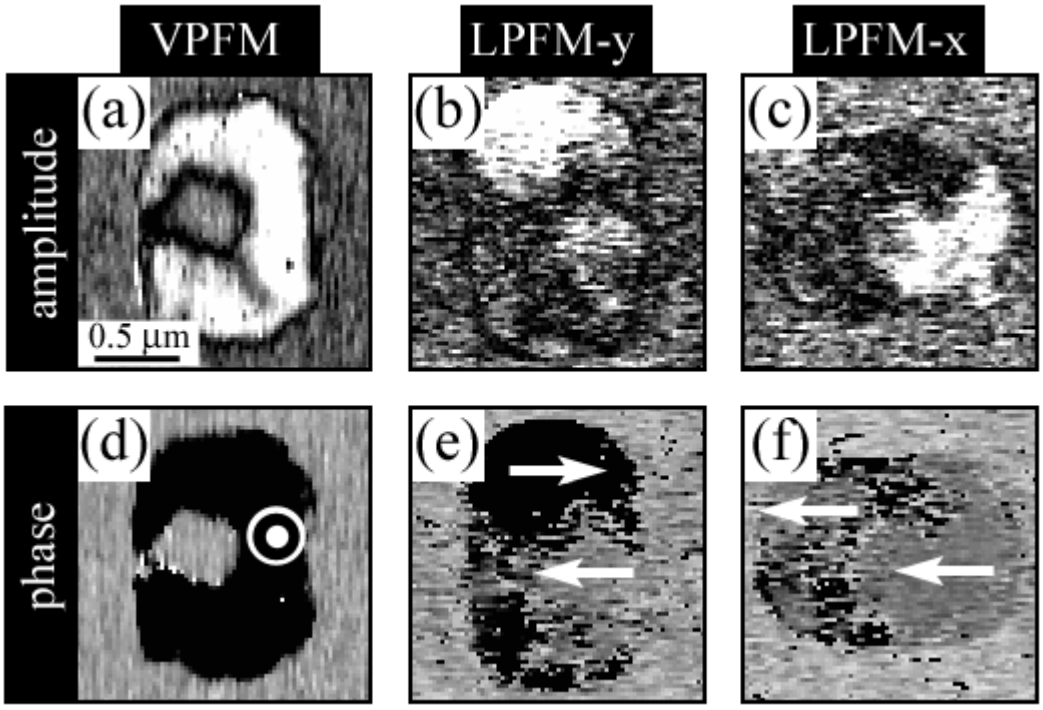

Fig. 2

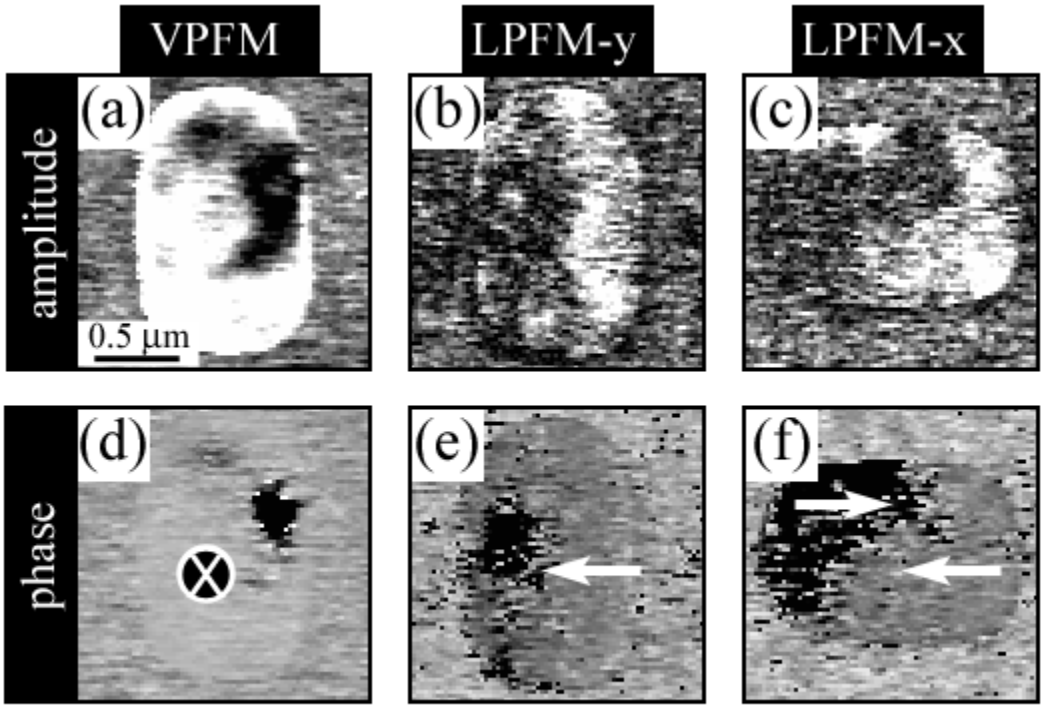

Fig. 3

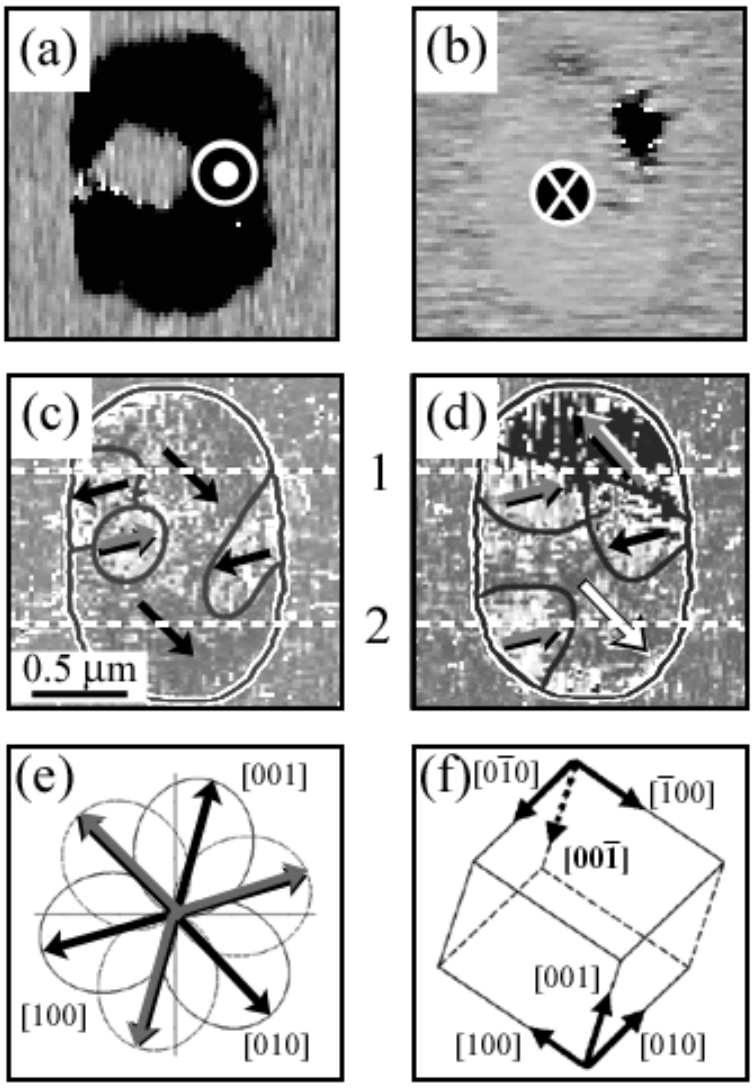

Fig. 4

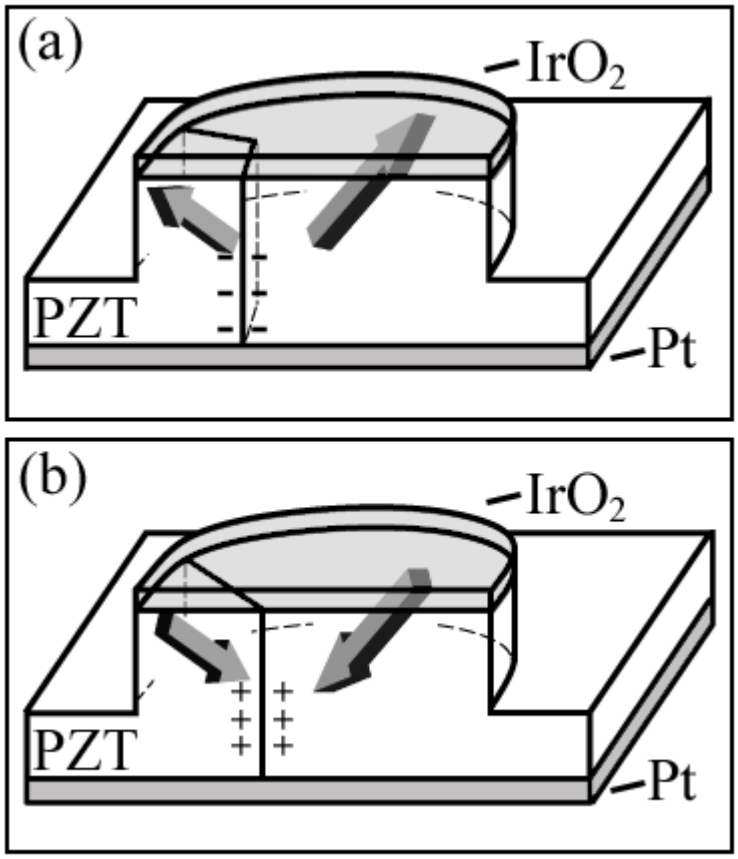

Fig. 5

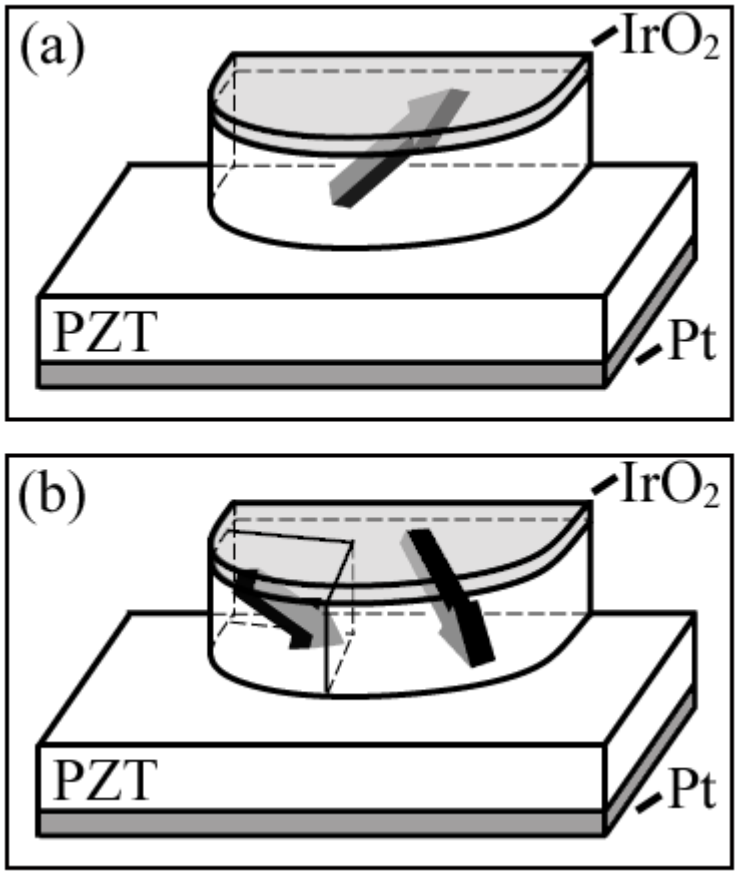

Fig. 6